Bulk and interfacial shear thinning of immiscible polymers

Sandra Barsky

Lawrence Berkeley National Laboratory and Department of Mathematics, University of California at Berkeley, Berkeley, California 94720

Mark O. Robbins

Department of Physics and Astronomy, Johns Hopkins University, Baltimore, Maryland 21218

Nonequilibrium molecular-dynamics simulations are used to study the shear-thinning behavior of immiscible symmetric polymer blends. The phase-separated polymers are subjected to a simple shear flow imposed by moving a wall parallel to the fluid-fluid interface. The viscosity begins to shear thin at much lower rates in the bulk than at the interface. The entire shear-rate dependence of the interfacial viscosity is consistent with a shorter effective chain length s^* that also describes the width of the interface. This s^* is independent of chain length N and is a function only of the degree of immiscibility of the two polymers. Changes in polymer conformation are studied as a function of position and shear rate. Shear thinning correlates more closely with a decrease in the component of the radius of gyration along the velocity gradient than with elongation along the flow. At the interface, this contraction of chains is independent of N and consistent with the bulk behavior for chains of length s^*. The distribution of conformational changes along chains is also studied. Central regions begin to stretch at a shear rate that decreases with increasing N, while shear induced changes at the ends of chains are independent of N.

I. INTRODUCTION

The viscosity of a polymer melt decreases when the melt is subjected to a sufficiently large shear rate, a phenomenon known as shear thinning. This non-Newtonian behavior is important in polymer processing and applications and has been extensively studied both experimentally and theoretically [1–3]. The basic origin of shear thinning is that polymers elongate and align with the flow when they are sheared more rapidly than they can relax. As the shear rate increases, the degree of alignment rises and the polymers present a decreasing hydrodynamic resistance to flow. Recent numerical simulations [4–8] have investigated a variety of issues in this non-Newtonian regime, including the shear-rate dependence of the viscosity, polymer conformation, and wall slip.

One area that has yet to be explored is shear thinning near the interface between immiscible polymers. Blending of polymers is common in industry, as this is one way of creating new materials. However, the blended polymers are often immiscible, leading to phase separation. The resulting interfaces can have a major impact on the processing and ultimate properties of the blend.

The static properties of interfaces in binary polymer blends are typically described by the Flory-Huggins model [9]. The degree of immiscibility is characterized by a parameter χ, which represents the free energy cost for placing a monomer of one type into a homogeneous region of the other type. There is a characteristic length s^* of the loops of one type of polymer that penetrate into the region occupied by the other polymer. By balancing the enthalpic cost and entropy gain, one finds that $s^* \sim 1/\chi$ [10]. The interface width scales as the radius of gyration of a segment of length s^*.

De Gennes and co-workers argued that the dynamic properties of the interface should also be controlled by s^* rather than the chain length N [10]. In particular, they suggested that for polymers in the Rouse limit the interfacial viscosity η_I should be given by the bulk viscosity of chains of length s^*. This implies that η_I is only a function of χ and has no dependence on N (as long it is larger than s^*). Goveas and Fredrickson reached similar conclusions from more detailed calculations [11].

In a recent paper, we presented a simulation study of the interfacial viscosity in the Newtonian regime of a symmetric binary blend of Rouse polymers [12]. As predicted [10,11], we found that the interfacial viscosity is determined by the degree of immiscibility and converges to a chain length independent value at large N. Moreover, both η_I and the interface width decrease with increasing immiscibility and their values are consistent with a common value of s^*.

In this paper, we investigate the shear-thinning behavior of the interfacial viscosity. We find that the same s^* that sets the width of the interface and the Newtonian viscosity determines the shear rate where shear thinning begins. Indeed the entire variation of η_I with shear rate follows the bulk shear-thinning curve for chains of length s^* and is independent of N. The shear-rate dependent viscosity converges to the bulk behavior for chains of length N at distances of order R_g from the interface. Since N is larger than s^*, the bulk viscosity η_B is higher than η_I in the Newtonian regime and begins to shear thin at a lower shear rate. Indeed, the interface does not begin to shear thin until η_B has decreased to a value that is comparable to the Newtonian limit of η_I. At higher shear rates the viscosity is nearly independent of distance from the interface.

We also examine changes in the conformational properties of chains near the interface and in the bulk as a function of shear rate. In equilibrium, the bulk values of the mean-square components of the end-to-end vector are equal, $R_x^2 = R_y^2 = R_z^2$. The two components in the plane of the interface (x and y) remain nearly unchanged at the interface, but the normal component decreases because of the constraint imposed

by immiscibility. As the shear rate is increased, polymers elongate along the direction of flow (x), and contract in the orthogonal directions. We find substantial elongation before there is any measurable change in bulk viscosity. The onset of bulk shear thinning appears to be more closely correlated with the onset of contraction in the z direction. The correlation between viscosity and contraction is even more dramatic at the interface. Like η_I, plots of R_z^2 as a function of shear rate are independent of N and follow the bulk behavior for chains of length s^*. In contrast, changes in elongation depend on N and begin at lower shear rates than changes in η_I.

The remainder of the paper is organized as follows. In the next section, we review the interaction potentials and simulation techniques used in this work. Results and analyses are described in Sec. III, and a summary and discussion are presented in Sec. IV.

II. MODEL

The polymer model and simulation techniques are similar to those used in previous work [12–14]. The polymer potential is based on the bead-spring model developed by Kremer and Grest [15]. Linear polymers containing N beads each are created by linking nearest neighbors on a chain with the potential

$$U_{nn}(r_{ij}) = \begin{cases} -\frac{1}{2}kR_0^2 \ln[1-(r_{ij}/R_0)^2], & r_{ij} < R_0 \\ \infty, & r_{ij} \geq R_0, \end{cases} \quad (1)$$

where r_{ij} is the distance between beads i and j, $R_0 = 1.5\sigma$, $k = 30\epsilon/\sigma^2$, and σ and ϵ set the length and energy scales, respectively. All particles in the system interact through a truncated Lennard-Jones potential

$$U_{LJ}(r_{ij}) = \begin{cases} 4\epsilon_{\alpha\beta}[(\sigma/r_{ij})^{12}-(\sigma/r_{ij})^6], & r_{ij} < r_{\alpha\beta}^c \\ 0, & r_{ij} \geq r_{\alpha\beta}^c, \end{cases} \quad (2)$$

where the interaction energy $\epsilon_{\alpha\beta}$ and cutoff $r_{\alpha\beta}^c$ depend on the types α and β of beads i and j, respectively. The cutoff is set at $r_{\alpha\beta}^c = 2^{1/6}\sigma$ to produce a purely repulsive interaction between beads. For interactions between polymers of the same type $\epsilon_{\alpha\alpha} = \epsilon$, with $\alpha = A$ or B. The two types of polymers are made immiscible [16] by increasing the repulsive energy between unlike beads to $\epsilon_{AB} = \epsilon_{BA} = \epsilon(1+\epsilon^*)$, where $\epsilon^* = 1.2$ or 3.2. Both values of ϵ^* are sufficient to produce phase separation for the range of chain lengths N considered here, $N = 16, 32,$ and 64.

The bounds of the simulation cell are periodic in the x and y directions, with periods $L_x \cong 38.5\sigma$ and $L_y \cong 33.4\sigma$, respectively. In the z direction the cell is bounded by top and bottom walls. Each contains $N_W = 3200$ atoms tied to the sites of a (111) plane of an fcc lattice by harmonic springs of stiffness $\kappa = 1320\epsilon/\sigma^2$. The walls are separated by $L_z \cong 47\sigma$. They confine 49 152 polymer beads, yielding a bead density of $\rho = 0.8\sigma^{-3}$ in regions far away from interfaces. Density oscillations are induced within a few σ of the walls [17]. However, the solid/polymer interfaces are only introduced to produce shear and are not of direct interest here. We thus restrict our discussion to regions more than five σ from the walls, where wall-induced ordering is negligible.

A symmetric blend is created in the following way. Polymers whose centers of mass are located in the bottom half of the simulation box are labeled type A and the remaining polymers are labeled B. The dividing plane is adjusted to ensure that there are equal numbers of polymers of each type. We also studied single phase systems with $N = 10$ and 14 at the same bead density.

Shear flow is induced by moving the top wall parallel to the interface at a constant speed v_W in the x direction. Due to the sharp wall/polymer interface and large polymer viscosity there can be a substantial difference between the velocities of the wall atoms and adjacent polymer beads [13,14,17–19]. We increased the wall/polymer interactions to limit this interfacial "slip," Atoms and beads interact through a Lennard-Jones potential with $\sigma_{WA} = \sigma_{WB} = \sigma$. For most simulations $\epsilon_{W\alpha} = \sqrt{1.7}\epsilon$ and the cutoff is extended to $r_{W\alpha}^c = \sqrt{1.5}\sigma$ to include part of the attractive region in the Lennard-Jones potential. At the highest shear rates studied, the wall/polymer interactions are increased by choosing $\epsilon_{WA} = \epsilon_{WB} = \sqrt{4.7}\epsilon$, and $r_c = \sqrt{2.5}\sigma$.

The equations of motion are integrated using a fifth-order predictor-corrector method [20], with a time step $\delta t = 0.0075\tau$, where $\tau = \sigma\sqrt{m/\epsilon}$ is the basic unit of time, and m is the mass of a monomer. A constant temperature of $k_BT = 1.1\epsilon$ is maintained with a Langevin thermostat [15]. To ensure that this thermostat does not bias the shear profile, the Gaussian white noise and damping terms are only added to the equations of motion for the velocity components normal to the mean flow (y and z) [13,21]. There is a characteristic time required for energy to flow from velocity fluctuations along the flow direction to the thermostatted components. When the inverse shear rate becomes comparable to this time, the kinetic energy along the flow direction is no longer thermostatted effectively. This limits the maximum shear rate in our simulations to about $0.2\tau^{-1}$. However, the correct ensemble for higher shear rates is a matter of continuing debate, and such strongly nonequilibrium states are not accessible to experiments [21,22].

The local shear rate $\dot{\gamma}$ of the fluid is easily calculated by taking the local rate of change in the x component of velocity, v_x as a function of z, i.e., $\dot{\gamma} = \partial v_x/\partial z$. This is done by taking slices parallel to the x-y plane, of width 0.095σ, and averaging the velocity of the monomers within these slices. The viscosity within a slice is found from

$$\eta = \frac{P_{xz}}{\dot{\gamma}}, \quad (3)$$

where the shear stress P_{xz} is constant throughout the system in steady state. Values of shear rate and viscosity presented below are averaged over ten slices.

The wall velocity is varied from $v_w = 0.1\sigma/\tau$ to $8.0\sigma/\tau$. As shown in Table I, this leads to a variation by almost two orders of magnitude in the bulk shear rate $\dot{\gamma}_B$ evaluated far from any interface. Note that this shear rate is the same in both fluids since we consider a symmetric melt. Statistical fluctuations drop with the total distance the wall moves and

TABLE I. Shear rate in bulk regions of each polymer $\dot{\gamma}_B$ at the indicated values of chain length and wall velocity v_W. Uncertainties are less than 5%. The proportionately larger shear rates at $v_W = 8\sigma/\tau$ are due to an increase in the wall-coupling parameters, as discussed in Sec. II.

u_W	$\dot{\gamma}_B$				
	$N=10$	$N=14$	$N=16$	$N=32$	$N=64$
0.1	0.0019	0.001 75	0.001 59	0.0013	0.000 94
0.3	0.0055	0.005 12	0.004 79	0.0039	0.0038
0.5	0.0091	0.008 72	0.0081	0.0074	0.0073
1.0	0.018	0.001 75	0.0171	0.0159	0.0166
2.0	0.037	0.036	0.0352	0.0360	0.0365
3.0	0.0563	0.0549	0.0538	0.0545	0.0554
5.0	0.093	0.0908	0.0899	0.0907	0.0943
8.0	0.171	0.168	0.168	0.166	0.171

increase with increasing chain lengths (e.g., Fig. 2). The simulations at lower shear rate were sheared for more than a million time steps after equilibration. Half this interval was used for higher shear rates.

III. RESULTS

A. Interface width

In Fig. 1, we show the densities of the two types of beads in the region near the interface for $\epsilon^* = 3.2$ and $N = 16$ and 64. For this strongly immiscible case, the densities change from their bulk values to zero over a few σ. Moreover, these density profiles are nearly unaffected when N is changed by a factor of 4 and the bulk shear rate is changed by a factor of 100.

Previous studies of equilibrium interfaces have related the interface width to the radius of gyration of polymer segments that enter the interfacial region [9–11,23,24]. The length of these segments s^* is determined by the degree of immiscibility and becomes independent of N in the large N limit. Earlier studies of the equilibrium properties of the model considered here [12] are consistent with these predictions. For example, for $\epsilon^* = 3.2$ the density profiles are indepen-
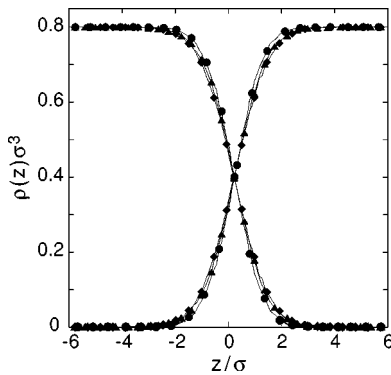
dent of N for $N \geq 16$. As illustrated in Fig. 1, this behavior extends to the highest shear rates studied here. The same insensitivity to shear rate is found for the less immiscible case of $\epsilon^* = 1.2$ where the interface is slightly wider.

B. Viscosity

The bulk viscosity of polymers whose length is shorter than the entanglement length can be described with Rouse theory [25]. The limiting Newtonian viscosity at low shear rates scales linearly with chain length: $\eta_B = \zeta b^2 \rho N$, where ζ is the monomeric friction coefficient and b is the statistical segment length. DeGennes and co-workers [10] argued that the viscosity in the interfacial region η_I should be determined by the effective length s^* rather than N because s^* is the length of segments that must relax during shear flow. Their conclusion is supported by the analysis of Goveas and Fredrickson [11] and by our earlier simulations in the Newtonian limit [12].

The dependence of the bulk and interfacial viscosities on chain length in the Newtonian limit is illustrated in Fig. 2. Here η is plotted against height z for $\epsilon^* = 3.2$ over the range of chain lengths where the interface width, and thus s^*, is constant. Away from the interface η approaches the bulk viscosity, which rises linearly with N for N up to 64. The slope of this rise determines $\zeta = 0.38 \pm 0.03 m/\tau$, since $b = 1.28\sigma$ is known from static properties [12,15] and $\rho = 0.8\sigma^{-3}$.
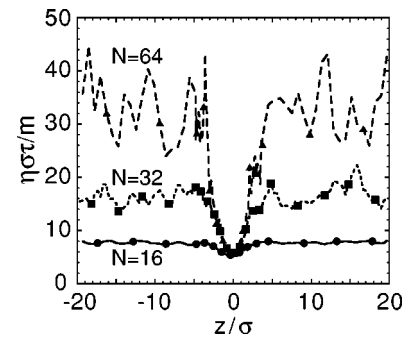

FIG. 1. Densities of type A (decreasing curves) and B (increasing curves) beads showing that the interface width is insensitive to chain length and shear rate. The immiscibility parameter is $\epsilon^* = 3.2$ and circles are for $N=64$, $v_W = 0.1$; diamonds are for $N = 64$, $v_W = 5.0$; and triangles are for $N-16$, $v_W = 5.0$. Corresponding values of $\dot{\gamma}_B$ are given in Table I.

FIG. 2. Newtonian viscosity as a function of height z for $\epsilon^* = 3.2$. The bulk viscosity scales linearly with chain length for $N = 16$ through 64, while the interfacial viscosity η_I is independent of chain length over this range.
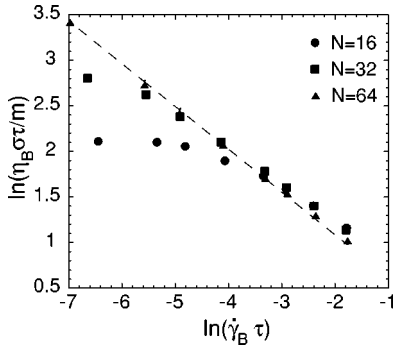
FIG. 3. Bulk viscosity η_B as a function of shear rate $\dot{\gamma}_B$, for polymers of length $N = 16$, 32, and 64. As N increases, shear thinning is observed at lower values of $\dot{\gamma}_B$. The dashed line shows a power law fit $\eta_B \sim \dot{\gamma}^{-0.47}$.

In the interfacial region the viscosity is smaller than the bulk value and is independent of chain length. This is consistent with the picture that the constant value of s^* determines η_I. Equating s^* to the chain length that would give a bulk viscosity equal to η_I yields $s^* \approx 10$. A similar analysis for $\epsilon^* = 1.2$ yields $s^* \approx 14$, and in both cases the radius of gyration corresponding to s^* is 1.6 times the interface width [12]. Thus, the Newtonian response is consistent with the picture advanced by deGennes and co-workers [10].

The shear-thinning behavior of the bulk viscosity with increasing shear rate is shown in Fig. 3. As is well known, the onset of shear thinning occurs when the system is sheared more rapidly than it can relax. Since the time to relax increases with chain length, the onset of shear thinning moves to lower shear rates with increasing N [7]. As in previous work [7], the decrease in viscosity at high shear rates can be fit to a power law $\eta \sim \dot{\gamma}^{-\alpha}$, with α near 1/2. The dashed line in Fig. 3 shows a fit to $N = 64$ data with $\alpha = 0.47$. The low shear-rate viscosity increases with chain length, and the high shear-rate behavior is nearly independent of N.

The variation of the interfacial viscosity with the interfacial shear rate is shown in Fig. 4 for different N and ϵ^*. In all cases, η_I begins to shear thin at much higher shear rates than η_B. Data is only presented for values of N where the Newtonian response and interface width are independent of chain length, so that s^* should also be constant. One sees from the figure that the shear-thinning behavior is also independent of N in this limit. Moreover, the entire shear-thinning curve for all N at each value of ϵ^* is consistent with the bulk shear-thinning behavior of chains with length equal to the values of s^* inferred from the corresponding Newtonian response. This is strong evidence that a single segment length determines the non-Newtonian shear-thinning behavior as well as the static interface profile and Newtonian response.

C. Polymer conformations

We now describe the changes in chain conformation that are associated with the shear thinning of the bulk and interface. Figure 5 shows the mean square of the three components of the end-to-end vector $\vec{R}$ as a function of the height
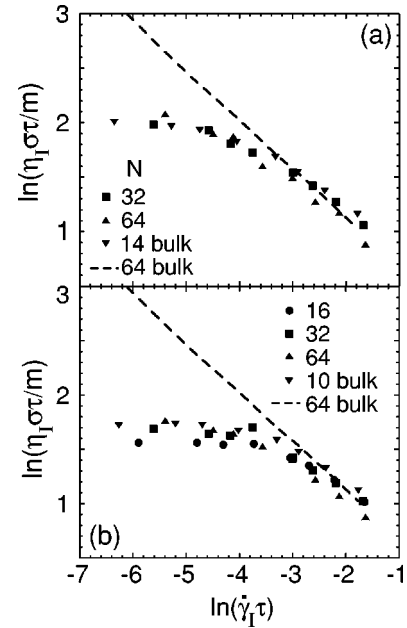

FIG. 4. Interfacial viscosity η_I as a function of interfacial shear rate $\dot{\gamma}_I$ for (a) $\epsilon^* = 1.2$ and $N = 32$ and 64, and (b) $\epsilon^* = 3.2$ and $N = 16$, 32, and 64. The bulk viscosities of polymers with length equal to the values of s^* determined from the Newtonian response are shown for comparison. The dashed lines show the bulk viscosity of chains of length 64. Interfacial shear rates are evaluated over an interval of width one σ in the center of the interface.

of the polymer's center of mass. The two panels show results for two low shear rates with $N = 16$ and $\epsilon^* = 3.2$. The lowest shear rate [Fig. 5(a)] is well into the Newtonian regime, and the polymers have time to relax to equilibrium conformations. Far from the interface the polymers follow isotropic
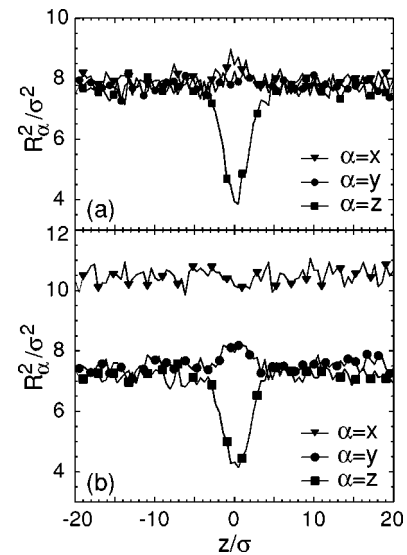

FIG. 5. Mean-square components of the end-to-end distance along $\alpha = x$, y, and z as a function of the center of mass height z for $N = 16$ polymers with $\epsilon^* = 3.2$ at (a) $v_W = 0.1\sigma/\tau$ and (b) $v_W = 0.5\sigma/\tau$. Although the viscosities at both shear rates are nearly indistinguishable from the limiting Newtonian viscosity, there is a clear stretching of polymers along the flow direction in (b).
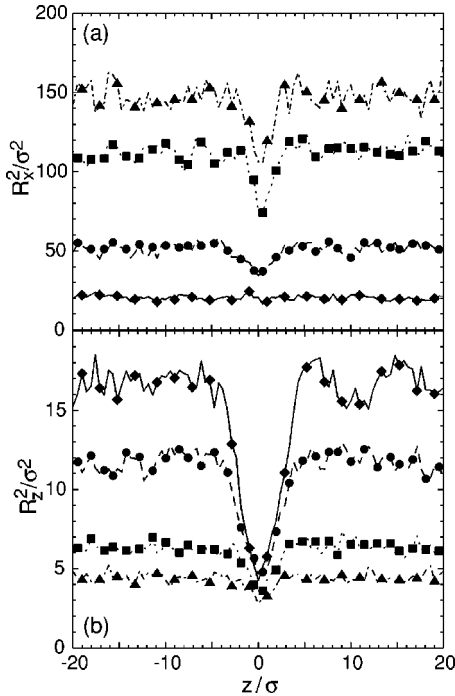
FIG. 6. Mean square x and z components of the end-to-end vector as a function of center of mass height for $N=32$ polymers at wall velocities $v_W=0.1\sigma/\tau$ (diamonds), $0.5\sigma/\tau$ (circles), $2\sigma/\tau$ (squares), and $5\sigma/\tau$ (triangles). Corresponding bulk shear rates are given in Table I.

FIG. 7. Mean-square z component of the end-to-end vector, R_z^2, for polymers centered at the interface with $N=16$, 32, and 64. Bulk values for chains with $N=10$ are shown for comparison. All curves begin to decrease at the same shear rate, and this shear rate coincides with the drop in interfacial viscosity.

random walks with $R_x^2=R_y^2=R_z^2\approx8\sigma^2$. Near the interface R_z^2 is strongly suppressed because immiscibility eliminates paths that take polymers too far into the other phase. The values of R_x^2 and R_y^2 are nearly unaffected by this constraint, but show a small rise that is comparable to our statistical noise. The value of R_z^2 does not attain its bulk level until the center of mass is far enough from the interface that chains are unlikely to reach it. This distance is comparable to the bulk value of $\sqrt{R_z^2}$, which is larger than the range over which the density changes (Fig. 1).

Figure 5(b) shows the mean-square components of $\vec{R}$ at the third lowest shear rate in Fig. 3. Surprisingly, although the viscosity is nearly indistinguishable from the low shear-rate limit, there is a substantial change in conformation. The component along the flow direction, R_x^2, increases by about 25% throughout the system. The bulk value of R_z^2 drops by about 10%, while the interfacial value is nearly unchanged. This is consistent with the observation that the interface shear thins at higher shear rates than the bulk.

Conformation changes at much higher shear-rates are illustrated in Fig. 6. Here the mean square x and z components of the end-to-end vector are plotted as a function of center-of-mass height for $N=32$, $\epsilon^*=3.2$, and four values of v_W. As expected, chains in the bulk regions are stretched and aligned along the flow direction. At the lowest shear rate, the bulk value of R_x^2 is about 20% above its equilibrium value. At the highest shear rate, the length of the polymer along the flow direction has grown to about 40% of the fully extended length. The components orthogonal to the flow decrease. The drop in R_z^2 is much larger than that in R_y^2, which drops from
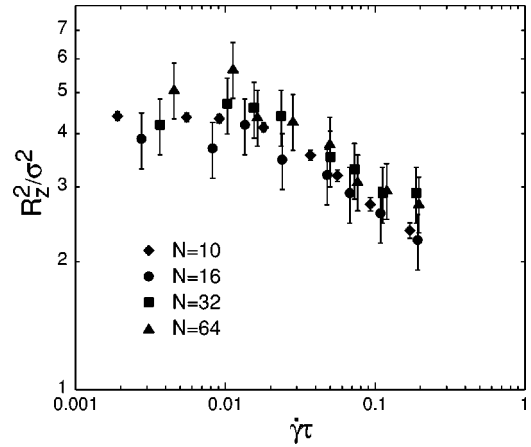
about 17 to $10\sigma^2$ over the studied range of $\dot{\gamma}$. Overall there is a net increase in R^2 from about 50 to $180\sigma^2$, because the increase in R_x^2 is much larger than the decrease in the other two components.

Chains in the interfacial region also stretch along the flow direction and contract in the orthogonal directions. However, as with the viscosity, the shear-rate dependence is shifted to higher $\dot{\gamma}$ at the interface. The value of R_x^2 is initially slightly higher at the interface and increases more slowly with $\dot{\gamma}$, leading to a pronounced dip at the highest shear rates. In contrast, the dip in R_z^2 at the interface decreases with increasing shear rate because the bulk value drops more rapidly with $\dot{\gamma}$.

Figure 7 provides a more detailed picture of the variation in the conformation of chains near the interface with increasing shear rate. Interfacial values of R_z^2 are plotted against shear rate for $N=16$, 32, and 64 at $\epsilon^*=3.2$. Bulk values for chains with length equal to the inferred value of $s^*=10$ are shown for comparison. All curves are flat at low shear rates, and begin to decrease at the point where the interfacial viscosity begins to fall in Fig. 4. As with the data for η_I, the interfacial conformations for all chain lengths collapse onto a universal curve that coincides with the bulk curve for chains of length s^* within our error bars. This provides further evidence that a single time scale corresponding to s^* controls the behavior of the interface. Note that the uncertainties are larger for interfacial values due to the relatively low number of polymers whose center of mass lies at the interface. As discussed previously [12,26], there is a preponderance of chain ends at the interface. This reduces the number of chain centers at the interface by a factor of 3 for the parameters considered here.

The idea that relaxation times should scale with the length of a subset of the chain rather than its entire length is related to other recent work [27]. These papers have examined changes in the conformation of individual chains pulled through gels or other polymers. Segments at the free end of the chain are assumed to relax with a time scale that is char-
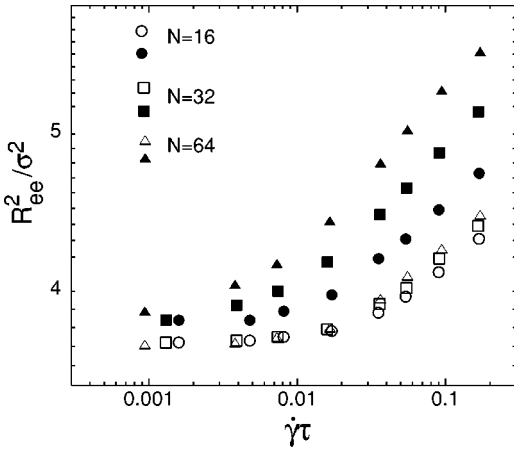
FIG. 8. Mean-square end-to-end distance of four bead segments at the middle (filled symbols) and ends (open symbols) of polymers with the indicated N as a function of shear rate. The ends show the same behavior for all N. The middles begin to stretch at a lower shear rate that decreases with increasing N.

acteristic of bulk polymers with the same length as the segment. Since the relaxation time grows with the length of the segment, the polymer is less relaxed and more stretched as one moves away from the free end toward the pulling end.

A similar phenomenon should occur within individual chains in a sheared polymer melt. Segments at the end of the chain will be more relaxed than the center leading to a dumbbell configuration that narrows in the center. In addition, the ends should begin to stretch at higher shear rates than the center because their characteristic relaxation time is shorter. Figure 8 shows the end-to-end distance of segments of length 4 as a function of shear rate. Results for the two end segments are averaged and compared to a segment in the middle of the chain. Note that the ends show the same behavior for all N indicating that the characteristic relaxation time for their conformations is only a function of segment length. In contrast, the middle segment becomes more stretched as N increases and the characteristic rate at which it can no longer relax decreases with increasing N. These effects are reminiscent of a nematic coupling effect seen recently in polymers, where the orientation of middle segments also relaxed more slowly with increasing N, while the rapid relaxation of ends was independent of N [28].

IV. SUMMARY AND DISCUSSION

In this paper, we have examined shear thinning and conformational changes in the bulk and interfacial regions of a phase-separated binary blend of Rouse chains. The bulk behavior is consistent with previous studies. The most surprising result is that pronounced elongation of the chains is observed before there is a noticeable change in viscosity. The onset of significant changes in η_B seems more closely connected to the contraction along the gradient direction, which becomes appreciable at higher shear rates than the elongation along the flow direction.

The changes in interfacial viscosity are consistent with the prediction [10,11] that the interfacial viscosity is determined entirely by the characteristic length s^* of loops that cross the

interface between immiscible polymers. This length is determined by the degree of immiscibility and independent of N for the polymers studied here. The interfacial viscosity shows these same trends with χ and N. For each degree of immiscibility, plots of interfacial viscosity against interfacial shear rate for different N collapse onto a single curve. The entire curve coincides with the bulk shear-thinning behavior of polymers of length 10 for $\epsilon^*=3.2$ and 14 for $\epsilon^*=1.2$. Thus a single effective chain length describes both the Newtonian value of η_I and its shear-thinning behavior. Our previous work showed that the same effective chain length described the width of equilibrium interfaces [12].

The suppression of the viscosity near the interface (Fig. 2) leads to an effective slip boundary condition [10–12]. The amount of slip is most pronounced in the Newtonian limit, where the difference between η_I and η_B is largest. As the bulk viscosity begins to shear thin, the amount of slip decreases. Once the shear rate is high enough to produce significant shear thinning at the interface, the bulk and interfacial viscosities converge (Fig. 4). In this limit the amount of slip is negligible.

Changes in the conformation of polymers near the interface were also studied. In equilibrium, the interface suppresses the component of the end-to-end vector perpendicular to the interface, but has little effect on the in-plane components. The changes in interfacial viscosity are most closely correlated with changes in the perpendicular component. Like η_I, plots of R_z^2 against shear rate for different chain lengths collapse onto a common curve that is consistent with that for bulk chains of length s^* (Fig. 7). While the elongation increases more slowly near the interface than in the bulk, it begins at much lower shear rates than the change in interfacial viscosity (i.e., Fig. 5) and depends on chain length. Thus, our results for both the bulk and interface indicate that polymer contraction perpendicular to the interface is the most important structural change associated with shear thinning.

We also explored changes in the conformation of segments of four beads within longer chains as a function of shear rate. Segments in the center of the chains began to elongate at the same shear rate where the bulk viscosity for the given chain length showed shear thinning. However, the conformation of the ends remained unchanged until much higher shear rates. Moreover, the conformation of the ends was nearly independent of the total chain length and their shear-thinning behavior was comparable to that for bulk chains with length 4. Recent studies of much longer chains have used the concept of a position dependent relaxation time to determine the conformation of a single chain in a solvent or gel [27]. Our study shows that the same concept applies to polymer melts.

[1] W. Carl, Macromol. Theory Simul. **3**, 705 (1994).

[2] F. Ganazzoli and A. Tacconelli, Macromol. Theory Simul. **7**, 79 (1998).

[3] A. N. Semenov, A. V. Subbotin, G. Hadziioannou, G. Ten Brinke, E. Manias, and M. Doi, Macromol. Symp. **121**, 175 (1997).

[4] T. W. Liu, J. Chem. Phys. **90**, 5826 (1989).

[5] J. J. López Cascales, S. Navarro, and J. García de la Torre, Macromolecules **25**, 3574 (1992).

[6] P. J. Daivis and D. J. Evans, J. Chem. Phys. **100**, 541 (1994).

[7] Z. Xu, J. J. de Pablo, and S. Kim, J. Chem. Phys. **102**, 5836 (1995).

[8] A. V. Lyulin, D. B. Adolf, and G. R. Davies, J. Chem. Phys. **111**, 758 (1999).

[9] P. Flory, *Principles of Polymer Chemistry* (Cornell University Press, Ithaca, 1953).

[10] P. G. de Gennes, C. R. Acad. Sci. Ser II; Mec., Phys. Chim., Sci. Terre Univers **308**, 1401 (1989); F. Brouchard-Wyart, P. G. de Gennes, and S. Troian, *ibid.* **310**, 1169 (1990); P. G. de Gennes, in *Physics of Surfaces and Interfaces*, edited by I. C. Sanchez (Butterworth-Heinmann, Boston, 1992).

[11] J. L. Goveas and G. H. Fredrickson, Eur. Phys. J. B **2**, 79 (1998).

[12] S. Barsky and M. O. Robbins, Phys. Rev. E **63**, 0211801 (2001).

[13] P. A. Thompson and M. O. Robbins, Phys. Rev. A **41**, 6830 (1990).

[14] P. A. Thompson and S. M. Troian, Nature (London) **389**, 360 (1997).

[15] K. Kremer and G. S. Grest, J. Chem. Phys. **92**, 5057 (1990).

[16] G. S. Grest, M.-D. Lacasse, K. Kremer, and A. M. Gupta, J. Chem. Phys. **105**, 10 583 (1996); M.-D. Lacasse, G. S. Grest, and A. J. Levine, Phys. Rev. Lett. **80**, 309 (1998).

[17] R. Khare, J. J. de Pablo, and A. Yethiraj, Macromolecules **29**, 7910 (1996).

[18] A. Jabbarzadeh, J. D. Atkinson, and R. I. Tanner, J. Chem. Phys. **110**, 2612 (1999).

[19] K. B. Migler, H. Hervet, and L. Leger, Phys. Rev. Lett. **70**, 287 (1993).

[20] M. Allen and D. Tildesley, *Computer Simulations of Liquids* (Oxford University Press, Oxford, 1987).

[21] M. J. Stevens and M. O. Robbins, Phys. Rev. E **48**, 3778 (1993).

[22] S. S. Sarman, D. J. Evans, and P. T. Cummings, Phys. Rep. **305**, 1 (1998).

[23] E. Helfand and Y. Tagami, J. Chem. Phys. **56**, 3592 (1971).

[24] H. Furukawa, Phys. Rev. A **40**, 6403 (1989).

[25] M. Doi and S. F. Edwards, *The Theory of Polymer Dynamics* (Clarendon, Oxford, 1986).

[26] E. Helfand, S. M. Bhattacharjee, and G. H. Fredrickson, J. Chem. Phys. **91**, 7200 (1989).

[27] F. Brochard-Wyart, Europhys. Lett. **23**, 105 (1993); **30**, 387 (1995); A. Adjari, F. Brochard-Wyart, P. G. de Gennes, L. Leibler, J.-L. Viovy, and M. Rubinstein, Physica A **204**, 17 (1994).

[28] S. Barsky and G. Slater, Macromolecules **32**, 6348 (1999).